

# Observation of Bifurcation Property of Radial Electric Field Using a Heavy Ion Beam Probe

A. Fujisawa, H. Iguchi, T. Minami, Y. Yoshimura, H. Sanuki, K. Itoh, M. Isobe, S. Nishimura, C. Suzuki, K. Tanaka, M. Osakabe, I. Nomura, K. Ida, S. Okamura, K. Toi, S. Kado, R. Akiyama, A. Shimizu, C. Takahashi, M. Kojima, K. Matsuoka, Y. Hamada, M. Fujiwara

National Institute for Fusion Science, Oroshi-cho, Toki, Japan 509-5292

e-mail: fujisawa@nifs.ac.jp

**Abstract:** Bifurcation nature of potential profile of a toroidal helical plasma is investigated in the Compact Helical System (CHS), using a heavy ion beam probe. The measurements reveal that there exist three main branches of potential profiles in electron cyclotron resonance (ECR) heated plasmas with low density of  $n_e \sim 0.5 \times 10^{13} \text{cm}^{-3}$ . The branches with higher central potential exhibit a rather strong radial electric field shear that should result in fluctuation reduction and formation of transport barrier. Lissajous expression is useful to extract the bifurcation characteristics of potential structure.

## 1. Introduction

The discovery of the H-mode in the ASDEX tokamak is the first experimental demonstration that toroidal plasmas are capable to show structural bifurcation resulting in the improved confinement [1]. This discovery has stimulated exploitation of other improved confinement regimes in tokamaks, such as recent reversed shear related modes [2-6]. A number of models have been presented to understand the bifurcation and transition into the improved confinement regimes with the transport barrier formation. One of the most predominant hypotheses is based on bifurcation in radial electric field ( $E_r$ ) shear and suppression of fluctuation-driven transport due to  $E_r$ -shear creation [7-11].

In contrast to tokamaks, bifurcation in radial electric field has been inherently expected for toroidal helical plasmas. According to neoclassical theories, the helical ripple diffusion in toroidal helical plasmas causes highly nonlinear dependence of radial electric field on thermal parameters such as temperature and density [12,13]. A heavy ion beam probe (HIBP) has been installed on CHS [14] in order to investigate the bifurcation nature of the radial electric field in a toroidal helical plasma [15,16]. The measurements show a variety of both spatial and temporal patterns of potential profile. In particular, a number of fascinating bifurcation phenomena, such as electric pulsation [17] and formation of internal transport barrier (ITB) [18] have been observed in electron cyclotron resonance (ECR) heated plasmas. The electric pulsation is a nonlinear oscillation that is regarded as successive transitions between bifurcated branches. The

finding of the ITB is quite important for fusion application. The formation mechanism of the transport barrier is associated with the bifurcation property of radial electric field.

The primary purpose of this paper is to introduce observation of bifurcation patterns or characteristics of potential profiles with discussion of its association with transport barrier. The potential profile varies with a corresponding thermal structural change according to supplies of heating power and particles. The observation leads us to a phenomenological view that the plasmas should have three main branches, which are simply expressed with Lissajous diagrams between time traces of line-averaged density and central potential. An important knowledge is obtained about existence of hysteresis that allows an efficient route to reach the improved confinement regime with lower ECR-heating power.

## 1. Experimental Set-up

The CHS is a heliotron/torsatron device whose major and minor radii are 1.0m and 0.2m, respectively. The magnetic field configuration has a rotational symmetry of 45-degree in the toroidal direction. Four pairs of poloidal coils are provided to modify the plasma shape and shift the magnetic axis. The maximum strength of magnetic field is 2T at present. The CHS owns co- and ctr-NBI systems and three gyrotron systems as heating apparatus; the frequency of two gyrotrons is 53.2GHz, and the other is 106GHz. The maximum power of NBI is approximately 1MW. Different heating schemes produce a wide variety of plasmas belonging to quite different regimes in plasma parameters, and allow investigation of behavior of the plasmas in various regimes of collisionality.

The experiments introduced in this paper are all performed on the magnetic configuration whose axis is located on  $R_{ax}=0.921\text{cm}$  with its strength of 0.88T. The ECR is exactly on the magnetic axis at the gyrotron frequency of 53.2GHz. The CHS device is equipped with an HIBP whose maximum energy is 200keV. The HIBP has a unique feature. In order to manage the complicated beam trajectory in the magnetic field of a toroidal helical device, an additional beam sweep system is set in front of the energy analyzer as well as on the accelerator side [15,16]. This method extends the observable range widely over almost the whole plasma region. The necessary beam energy to observe this configuration is 72keV when cesium beam is used.

The HIBP is operated in two manners. The first one is to scan radial position by sweeping the beam trajectory continuously in order to obtain the potential profile. Time evolution of potential profile can be acquired in every a few millisecond at the fastest. The second one is that the beam orbit, or observation point, is fixed in order to investigate dynamics or fluctuation of plasma. The uncertainty of the absolute value of potential is mainly determined by the precision of accelerator and analyzer voltages. Difference in potential between two radial points, in principle, has no uncertainty. There is no ambiguity, therefore, to deduce the radial

electric field that is evaluated by difference of adjacent potentials.

## 2. Patterns of Potential Profile and Bifurcation Diagram

Experiments have been conducted in order to investigate how the potential profile changes according to density under a fixed ECR-heating power. The measurements are performed in hydrogen plasmas with only ECR heating whose power is fixed at  $P_{\text{ECRH}} \sim 100\text{kW}$ . The line-averaged density to be surveyed ranges from  $n_e \sim 0.2 \times 10^{13}\text{cm}^{-3}$  to  $n_e \sim 1.2 \times 10^{13}\text{cm}^{-3}$ . The other plasma parameters vary with the line-averaged density; for example, electron temperature decreases with an increase in density. The line-averaged density measured with an HCN laser interferometer is regarded here as a parameter to represent characteristics of the plasmas.

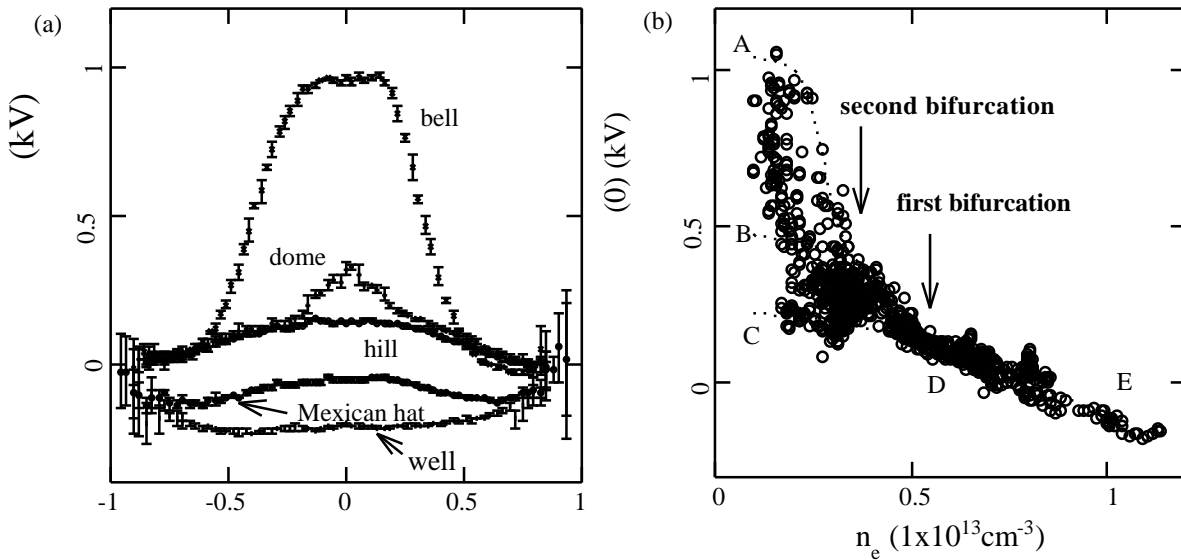


FIG.1: (a) Characteristic shapes of potential profiles that have been ever observed in CHS. The shapes are termed here bell, dome, hill, Mexican hat, and well-shape. (b) The central potential is a function of the line-averaged density in the case of ECR heating power of 100kW. In low-density regimes, bifurcation of the potential profile is observed at two critical values of density. Representative shapes of potential profiles are identical for five regimes. Only the well pattern has been found in the NBI heated plasmas, while all kinds of potential profiles have been identified in ECR-heated plasmas.

In the ECR-heated plasmas, it has been found that a variety of potential profiles exist as the line-averaged density changes. So far, the potential profile has been empirically classified into five patterns, as is illustrated in Fig. 1a. The patterns are termed *bell*, *dome*, *hill*, *Mexican-hat* and *well* in order from the higher to the lower central potential value. The higher potential states such as dome and bell are obtained as the ECR-heating power becomes higher with a fixed

density, or as the density becomes lower with a fixed ECR-heating power.

Figure 1b shows the central value of the measured potential profiles as a function of line-averaged density. The central potential values are evaluated for the potential profile measured in every 2-3ms in discharges. The present diagram has two critical values of density where the property of the potential profile changes drastically. Below the first critical density of  $n_e \sim 0.5 \times 10^{13} \text{cm}^{-3}$  (first bifurcation point), there higher potential value of  $\sim 0.4 \text{kV}$  is obtained in some shots. As density decreases further beyond the second critical value of  $n_e \sim 0.3 \times 10^{13} \text{cm}^{-3}$  (second bifurcation point), the potential value often reaches  $\sim 1 \text{kV}$ .

Three dashed lines are drawn to divide the diagram into the regions where the plasma shows characteristic shapes or patterns in potential profile. In the region (C) along the bottom dashed line with density of  $n_e \sim 0.5-0.6 \times 10^{13} \text{cm}^{-3}$ , the shape of potential profiles is consistent with the hill-shape. Below the first critical density along the middle dashed line (region-B), the most of measured potential profiles are identical with the dome around the core. Below the second critical density along the top dashed line (region-A), the profiles take the characteristic of the bell-shape; it can be interpreted as that the foot-point of the dome at  $\sim 0.3$  moves to the outer radius of  $\sim 0.5$ . The profiles of hill, dome and bell are recognized as bifurcated states in low-density regimes. One of the simple proofs is given by a time evolution of central potential, which shows pulsating behavior [19].

As the density increases from  $n_e \sim 0.6 \times 10^{13} \text{cm}^{-3}$  to  $n_e \sim 1.2 \times 10^{13} \text{cm}^{-3}$  along the bottom dashed line (region-D), the radial electric field in the periphery becomes negative with keeping positive around the core. Then the potential profile exhibits Mexican-hat feature. As the density further increases and becomes close to the density limit (region-E), the central positive value turns almost zero or slightly negative. The potential takes well-shape. Along the dashed line of  $n_e > 0.5 \times 10^{13} \text{cm}^{-3}$ , the profile shapes change gradually from Mexican hat to the well-shape.

The profiles of bell and dome are quite important for fusion application since these profiles possess rather large  $E_r$ -shear, that could result in formation of transport barrier. It is confirmed, in fact, that electron thermal transport barrier is established at the radius of the maximum  $E_r$ -shear for the ECR-heated plasma where the dome feature is stably maintained. At the position of the maximum  $E_r$ -shear, the density fluctuation is observed to reduce by approximately 50%. The gradient of electron temperature at the barrier position  $\sim 0.3$  increases from  $0.12 \text{keV/cm}$  (the value of the gradient of the plasma with hill feature) to  $0.57 \text{keV/cm}$ .

On the other hand, the confirmation has not been done for the plasmas with bell feature owing to the following reasons. i) The region where such plasmas can be maintained for a sufficiently long time has not been found in the experiments to date. ii) The plasma with bell feature is obtained in quite low-density where the Thomson scattering light is so poor to deduce electron temperature with sufficient precision.

Figure 2 shows deduced  $E_r$  and  $E_r$ -shear profiles in examples of bell and dome potential profiles. As is shown in Figs. 2b and 2c, the radial electric field around the connection layer is obtained by fitting a function form of  $\tanh[(r - r_0)/\Delta r]$  to the measured data. The estimation yields the maximum value of  $E_r$ -shear of  $\sim 60\text{V/cm}^2$  at  $r \sim 0.5$  for the bell profile, which is equivalent to that of the dome profile of  $\sim 40\text{V/cm}^2$  at  $r \sim 0.3$ . It is expected, therefore, that the internal transport barrier may be established for the plasmas with bell feature.

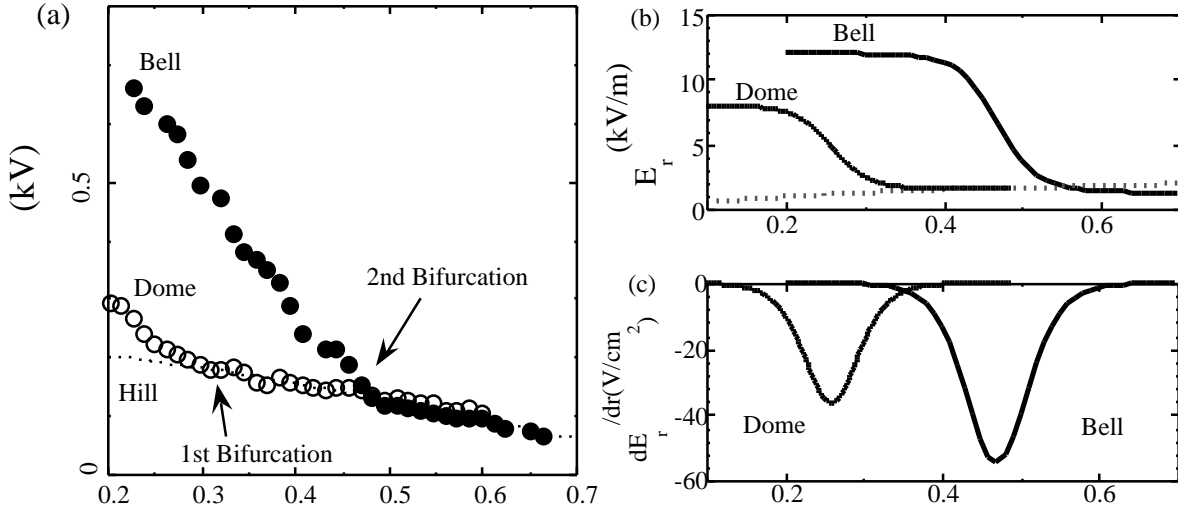


FIG.2: (a) Potential profiles with a discrete change in radial electric field. The hill pattern is shown for reference. (b) Profiles of radial electric field for dome and hill patterns. (c) Profiles of radial electric field shear for dome and hill patterns.

### 3. Evolution of Potential and Bifurcation Branches - Existence of Hysteresis

Our empirical knowledge has led us to a hypothesis that three branches of potential profile should exist in a low-density regime of the ECR-heating plasma. The hypothesis can be confirmed in evolution of potential profile when the ECR-heating is applied on the NBI-heated plasmas. Examples are provided here for this purpose in the following discharges where the ECR-heating of  $P_{\text{ECRH}} \sim 100\text{kW}$  is applied to the target NBI-heated plasmas with different densities.

Figure 3 shows four examples of time evolution of the central potential and the line-averaged density in deuterium plasmas. The plasmas in sequential shots have different initial densities that make their potential evolution quite different after the launch of ECR-heating. The initial densities of the plasmas are (A)  $n_e \sim 0.2 \times 10^{13} \text{cm}^{-3}$  (B)  $n_e \sim 0.6 \times 10^{13} \text{cm}^{-3}$ , (C)  $n_e \sim 0.8 \times 10^{13} \text{cm}^{-3}$  and (D)  $n_e \sim 0.9 \times 10^{13} \text{cm}^{-3}$ . It is clear that the initial increasing rate of potential is larger as the target density becomes lower. In the lowest density discharge (#76639), the line-averaged density

monotonically increases after launch of ECR-heating, while the other two shots show an increase in the density after an initial decrease. After that stage ( $90\text{ms} < t < 110\text{ms}$ ), the potential in shots #76640 and #76641 relaxes to a constant value that the potential of case #76642 takes.

In the cases with lower densities (#76639-#76641), the potential evolves with transitions from lower to the upper states in the earlier stage of discharges, while the potential value in shot #76642 alters monotoniously with a change in density. In the discharge with the lowest density shot #76639, back-and-forth transitions occur around  $t=52\text{ms}$  between dome and bell. In the other two shots (#76640 and #76641), the transitions from hill to dome take place at  $t\sim 60\text{ms}$  and  $t\sim 65\text{ms}$ . By using a fitting function of  $\tanh[(t-t_0)/\tau]$ , the time scale of these transitions is estimated about  $60\mu\text{s}$  for both shots (#76640 and #76641).

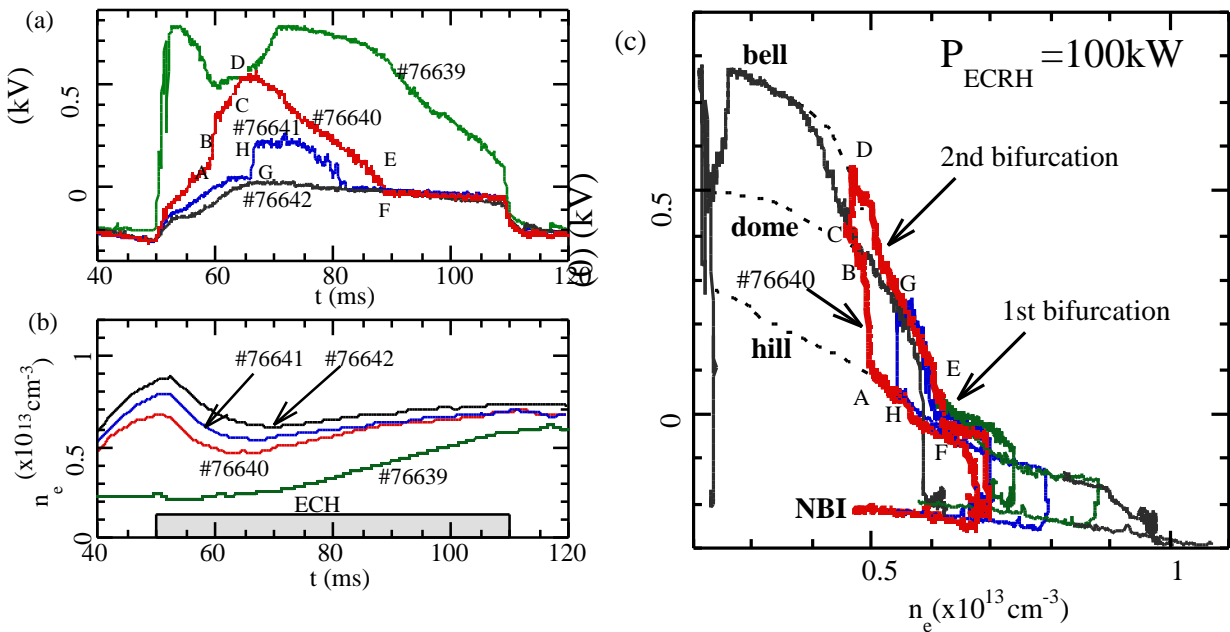


FIG.3: Evolution of the potential and the line-averaged density in plasmas with a combined heating of ECR (100kW)+NBI (800kW). (a) The waveforms of the central potential and (b) the line-averaged electron density. (c) The Lissajous lines made of the central potential and the line-averaged electron density. A clear hysteresis is seen; a clear difference in the density at which back- and forth transitions happen. Three distinctive branches exist for the combined phase of the ECR+NBI heating, while the NBI phase has only one branch

Characteristics of potential evolution, or bifurcation property, can be extracted by making a Lissajous diagram on potential evolution as a function of the line-averaged density. Figure 3c shows five Lissajous traces including the above four cases; the initial density of the rest is  $n_e \sim 1.2 \times 10^{13} \text{ cm}^{-3}$ . These Lissajous traces fall on curves indicating four branches; three branches in the combined heating phase of ECR+NBI and one for the NBI-heating phase. The potential profiles on three branches in this combined heating phase exhibit hill, dome and bell-

features shown in Fig. 1. On this bifurcation diagram, two critical density values of  $n_e \sim 0.5 \times 10^{13} \text{cm}^{-3}$  and  $n_e \sim 0.6 \times 10^{13} \text{cm}^{-3}$  are identical, where the gradient of curves is altered. These critical values are different from the values of the corresponding diagram for mere ECR-heated plasmas (see Fig. 1). This reason should be ascribed to the ion temperature difference owing to the NBI-application.

The Lissajous diagram also reveals a *hysteresis* in potential on the density evolution. As for the Lissajous traces of shot #76640, the plasma status evolves as a loop of A-B-C-D-E-F during the combined heating phase. Initially after launch of ECR-heating, the potential increases through point-F along the hill-branch. At point-A, the plasma status becomes unstable, then transition occurs from the hill- to the dome-branch. Similarly, the transition from the dome-branch to the bell-branch occurs at point-C. Then the plasma goes back to the dome-branch in a confinement time scale, and potential gradually decreases along the line of the dome-branch. Finally, back transition from the dome- to the hill-branch occurs at point-E to F. Clear hysteresis loops, therefore, exist for relationship between potential and density evolution. Also hysteresis and transition from the hill- to the dome-branch (from point H to G) are seen in the Lissajous trace of shot #76641.

#### 4. Discussion and Summary

For data set used in Fig. 1b with the low-ECR heating power of 100kW, the appearance of dome and bell-branches is very rare, compared to the realization of hill-branch. As the heating power increases, the probability for plasmas to take the higher potential branches (dome or bell) increases. The other experiments imply that the power threshold for the dome-feature should be  $P_{\text{ECRH}} \sim 150 \text{kW}$  for the plasmas with the line-averaged density of  $n_e \sim 0.4 \times 10^{13} \text{cm}^{-3}$ ; the potential profile with the dome feature has been empirically observed with a high probability in that condition. As the heating power further increases up to  $\sim 200 \text{kW}$ , the potential profile with the bell-feature can turn to appear, being accompanied with pulsation behavior.

Using the hysteresis, transition into higher potential states, or formation of the internal transport barrier is more easily realized in a lower density region. The realization probability of dome and bell-branches is actually larger, as is read in Fig. 1, in the lower density region. The scaling of energy confinement time for stellarators shows favorable dependence on line-averaged density [20];  $\tau_E \propto n_e^{0.59}$ . It is expected, accordingly, that higher density should be consistent with higher stored energy under the condition that the plasma potential (or other parameters) changes along a curve of an identical branch. Therefore, it is an effective route for achieving higher plasma performance to increase the density after making transition from hill-branch to dome-branch (or bell-branch) at a low density.

In summary, there exist three main bifurcated branches (hill, dome and bell) in potential

profiles in the ECR-heated plasmas in low-density regimes. In the dome-branch, the formation of the internal transport barrier around  $\rho \sim 0.3$  is confirmed for electron thermal energy. Lissajous expression is a useful method to extract bifurcation characteristics. A Lissajous diagram indicates a clear hysteresis giving an efficient route to achieve a better confinement regime with an internal transport barrier. To find an operational condition where the bell-branch is stably realized is an important future work since the branch can be associated with an internal transport barrier located at outer radius of  $\rho \sim 0.5$  resulting in higher plasma performance.

## References

- [1] Wagner F. et al., Phys. Rev. Lett. **49** (1982) 1408.
- [2] Lazarus E.A., Navratil G. A., Greenfield C. M., *et al.*, Phys. Rev. Lett. **77** (1996) 2714.
- [3] Levinton F. M., Zarnstorff M. C., Batha S. H., *et al.*, Phys. Rev. Lett. **75** (1995) 4417.
- [4] Fujita T., Ide S., Shirai H., Kikuchi M., Naito O., Koide Y., Takeji S., Kubo H., Ishida S., Phys. Rev. Lett. **78** (1997) 2377.
- [5] Erckmann V., Wagner F., Baldzuhn J. *et al.*, Phys. Rev. Lett. **70** (1993) 2086.
- [6] Toi K., Okamura S., Iguchi H. *et al.*, *Proceedings of 14th International Conference on Plasma Physics and Controlled Nuclear Fusion Research*, Wurzburg, 1992, (International Atomic Energy Agency, Vienna, 1993), **Vol. 2**, p. 461.
- [7] For review, Itoh K., Itoh S.-I., Phys. Contr. Fusion **38** (1996)1. Itoh K., Itoh S. -I., Fukuyama A., Transport and Structural Formation in Plasmas, ed. P. Scott and H. Wilhelmsson, (Bristol and Philadelphia, Institute of Phys. Pub.).
- [8] Itoh S.-I., Itoh K., Phys. Rev. Lett., **60** (1988) 2276.
- [9] Shaing K. C., Crume, Jr. E., Phys. Rev. Lett., **63** (1989) 2369.
- [10] Groebner R. J., Burrell K. H., Niedermayer H. et al., Phys. Rev. Lett. **64** (1990) 3015.
- [11] Ida K., Hidekuma S., Miura Y. et al., Phys. Rev. Lett. **65** (1990) 1364.
- [12] Hastings D. E., Houlberg W. A., Shaing K. C., Nucl. Fusion **25** (1985) 445.
- [13] Kovrizhnykh L. M., Nucl. Fusion **24** (1984) 435.
- [14] Matsuoka K., Kubo S., Hosokawa M., et al., in Plasma Physics and Controlled Nuclear Fusion Research 1988(Proc. 12th Int. Conf. Nice, 1988), International Atomic Energy Agency, Vienna, 1989, **Vol. 2**, 411.
- [15] Fujisawa A., Iguchi H., Sasao M., Hamada Y., Fujita J., Rev. Sci. Instrum. **63** (1992) 3694.
- [16] Fujisawa A., Iguchi H., Lee S. et al., Rev. Sci. Instrum. **67** (1996) 3099.
- [17] Fujisawa A., Iguchi H., Idei H., et al., Phys. Rev. Lett. **81** (1998) 2256.
- [18] Fujisawa A., Iguchi H., Minami T., et al. Phys. Rev. Lett. **82** (1999) 2669.
- [19] Fujisawa A., Iguchi H., Minami T., et al. Plasma Phys. Control. Fusion **42** (2000) A103.
- [20] Stroth U., Murakami M., Yamada H., et al., Nucl. Fusion **36** (1996) 1063.